Supporting Information

Colloidal Ni-Co-Sn Nanoparticles as Efficient Electrocatalysts for the Methanol Oxidation Reaction

Junshan Li,[a,b] Zhishan Luo,[a,*] Feng He,[c,d,*] Yong Zuo,[a,b] Chaoqi Zhang,[a,b] Junfeng Liu,[a,b] Xiaoting Yu,[a,b] Ruifeng Du,[a,b] Ting Zhang,[e] Maria F. Infante-Carrió,[e] Pengyi Tang,[e] Jordi Arbiol,[e,f] Jordi Llorca,[g] Andreu Cabot [a, f,*]

a Catalonia Institute for Energy Research - IREC, Sant Adrià del Besòs, Barcelona, 08930, Spain

b Departament d'Electronica, Universitat de Barcelona, 08028 Barcelona, Spain

c Key Laboratory of Organic Solids, Institute of Chemistry, Chinese Academy of Sciences, Beijing 100190, PR China.

d University of Chinese Academy of Sciences, Beijing 100049, P.R. China.

e Catalan Institute of Nanoscience and Nanotechnology (ICN2), CSIC and BIST, Campus UAB, Bellaterra, 08193 Barcelona, Spain

f ICREA, Pg. Lluís Companys 23, 08010 Barcelona, Spain

g Institute of Energy Technologies, Department of Chemical Engineering and Barcelona Research Center in Multiscale Science and Engineering. Universitat Politècnica de Catalunya, EEBE, 08019 Barcelona, Spain

Corresponding Author

* Andreu Cabot: acabot@irec.cat

* Zhishan luo: luozs@mail.sustc.edu.cn

* Feng He: hefeng2018@iccas.ac.cn

Contents

Additional TEM micrograph

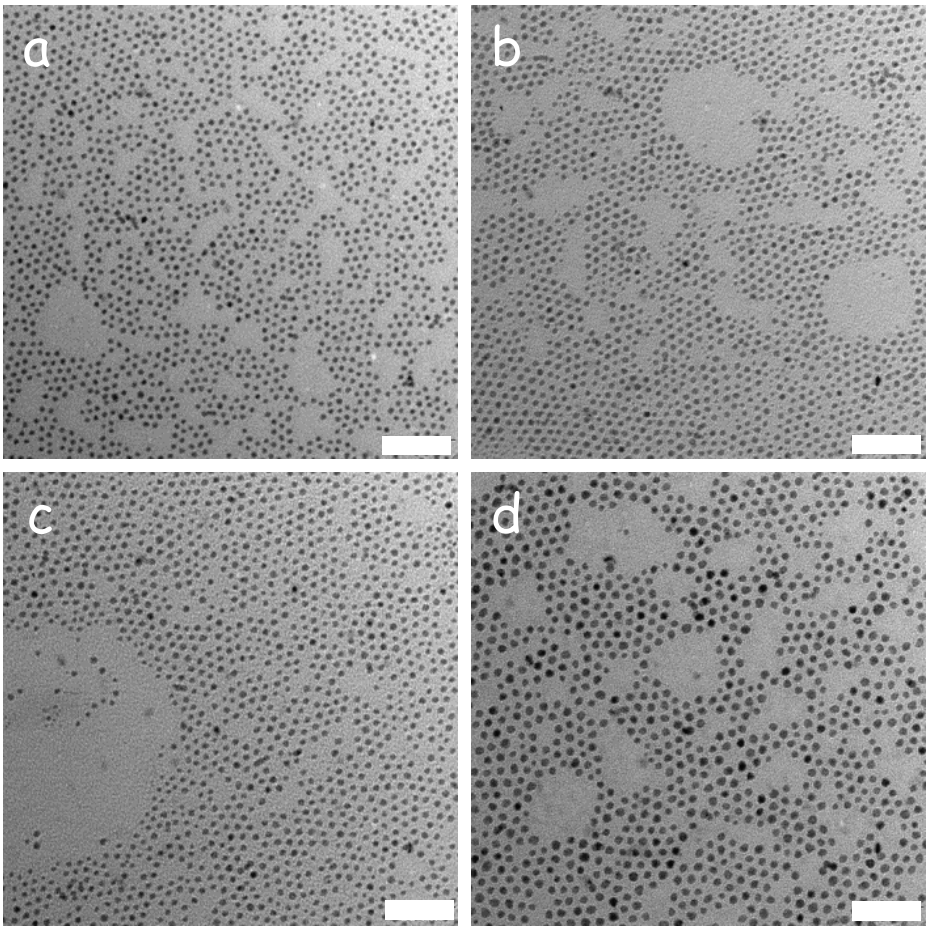

Figure S1. Representative TEM micrographs of $Ni_{3-x}Co_xSn_2$ NPs with different Co contents: a) x = 0.5, b) x = 1.0, c) x = 2.0, d) x = 2.5. Scale bar: 50 nm.

SEM-EDX characterization

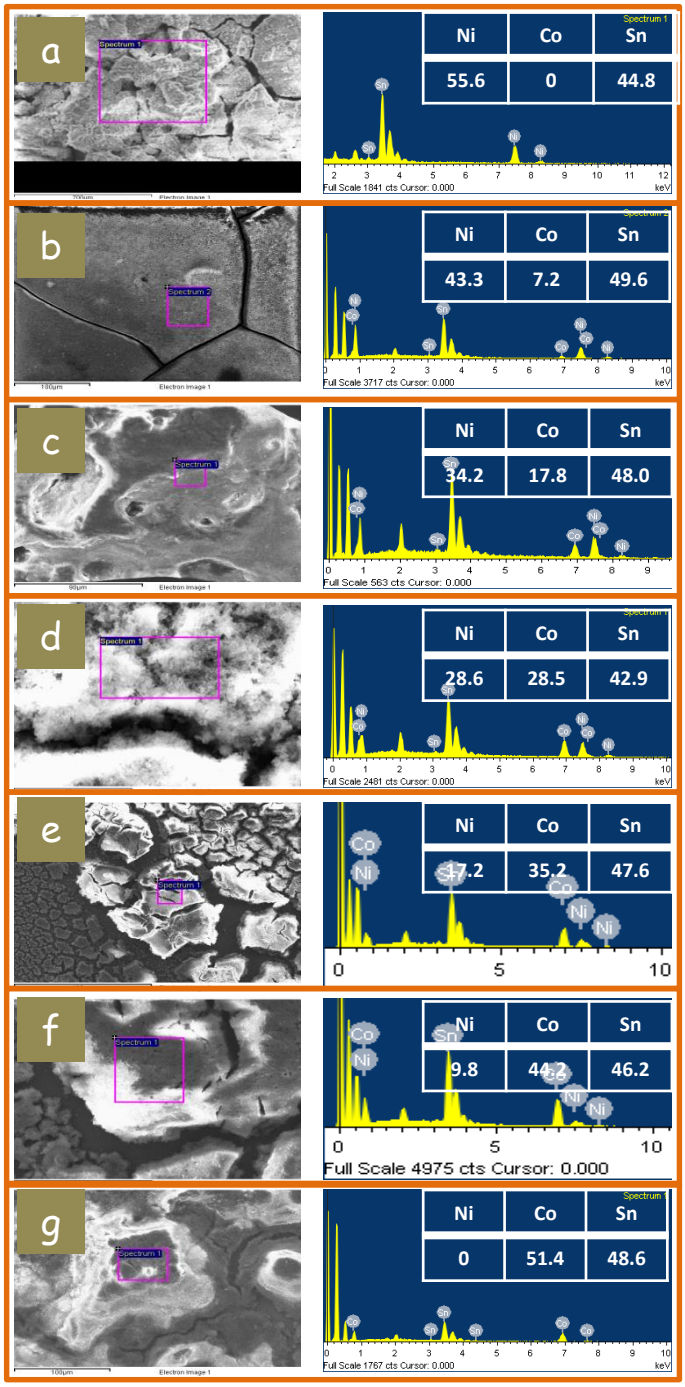

Figure S2. SEM-EDX characterization of the NPs of $Ni_{3-x}Co_xSn_2$: a) x = 0, b) x = 0.5, c) x = 1.0 d) x = 1.5, (e) x = 2.0, f) x = 2.5, g) x = 3.0. In the table, weight percentage for each metal was used.

HRTEM micrographs

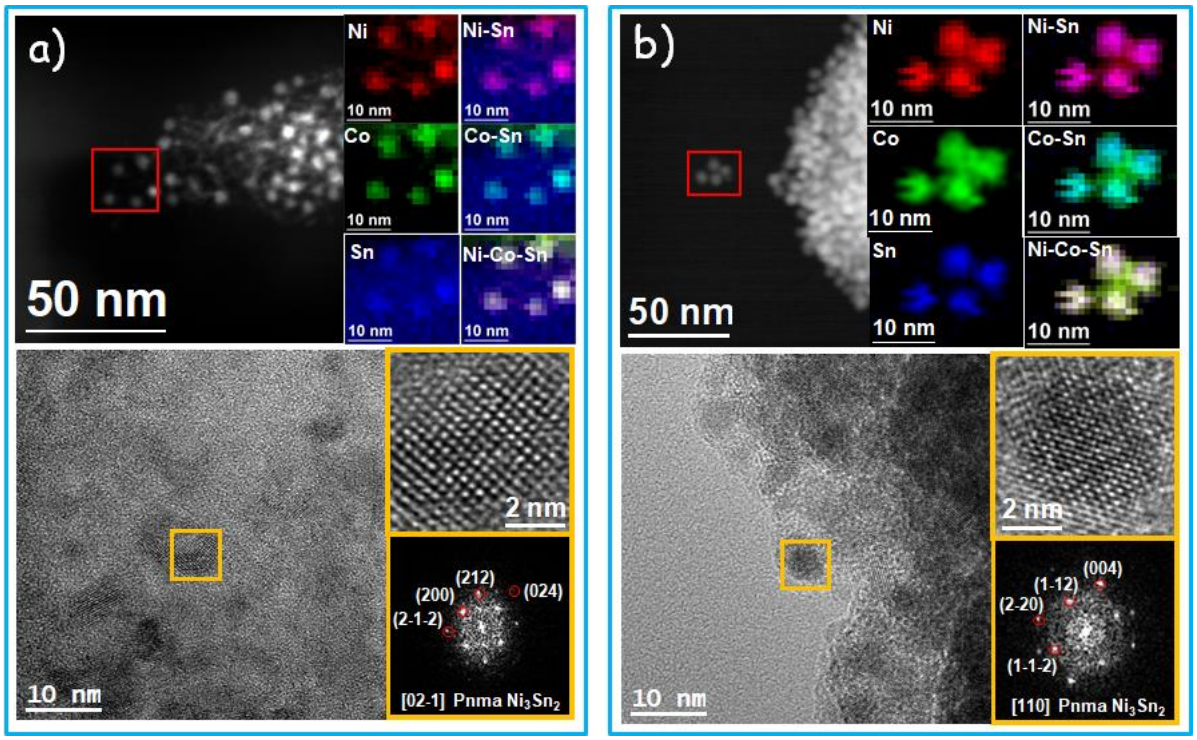

Figure S3. HRTEM micrograph and ADF-STEM image and EELS elemental mapping of $Ni_{3-x}Co_xSn_2$: a) x = 1.0, b) x = 1.5.

XPS characterization

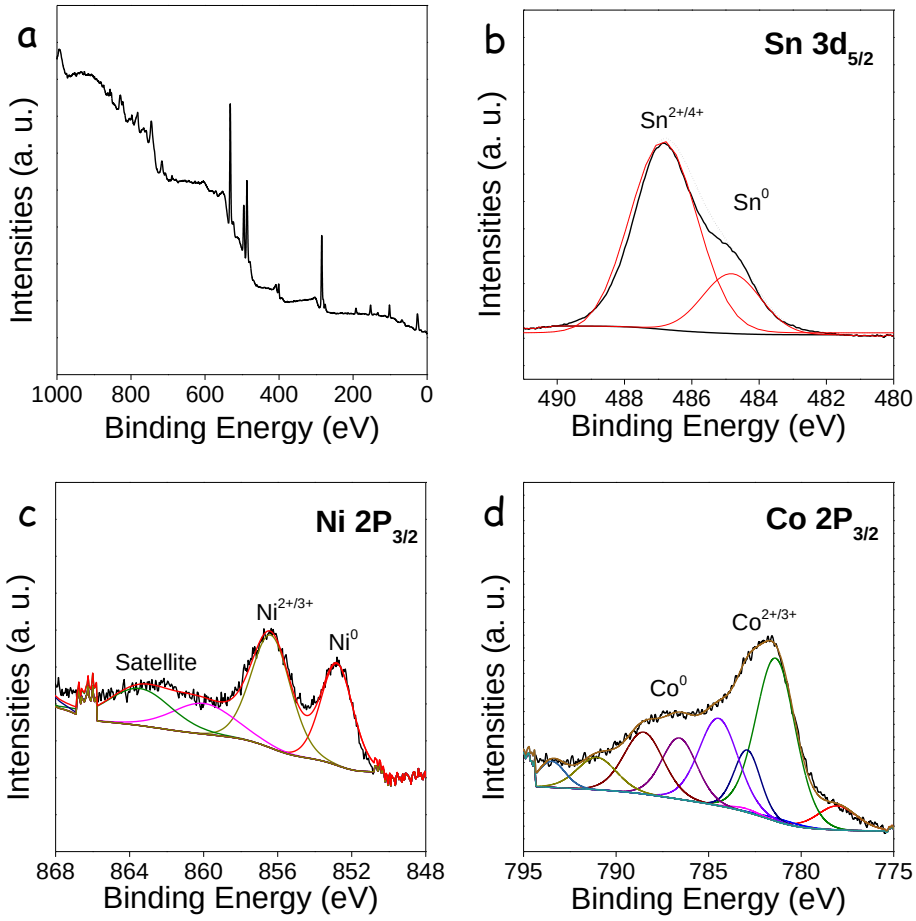

Figure S4. XPS spectra of $Ni_{3-x}Co_xSn_2$ (x = 1.5) NPs.

Ni is presented at the NPs surface in two different chemical states, which we associated to metallic Ni^0 (852.8 eV) and $Ni^{2+/3+}$ chemical environment (856.4 eV).[1] An additional satellite peak was also observed at 863.4 eV. The fitting peaks of 778.0 eV， 781.0 eV and 783.0 eV are indexed to metallic Co and oxides, respectively.[1] The amount of Co^0 is smaller than that of $Co^{2+/3+}$. In addition, two tin chemical states were identified from the XPS analysis of the Sn $3d_{5/2}$ electronic states. A Sn $3d_{5/2}$ peak at higher binding energy, 486.8 eV was assigned to an oxidized environment.[1] A second Sn $3d_{5/2}$ peak at 484.8 eV matched with the binding energy expected from Sn in a metallic environment, thus we related it to the Sn within the $Ni_{3-x}Co_xSn_2$ alloy.[1]

Ligand removal

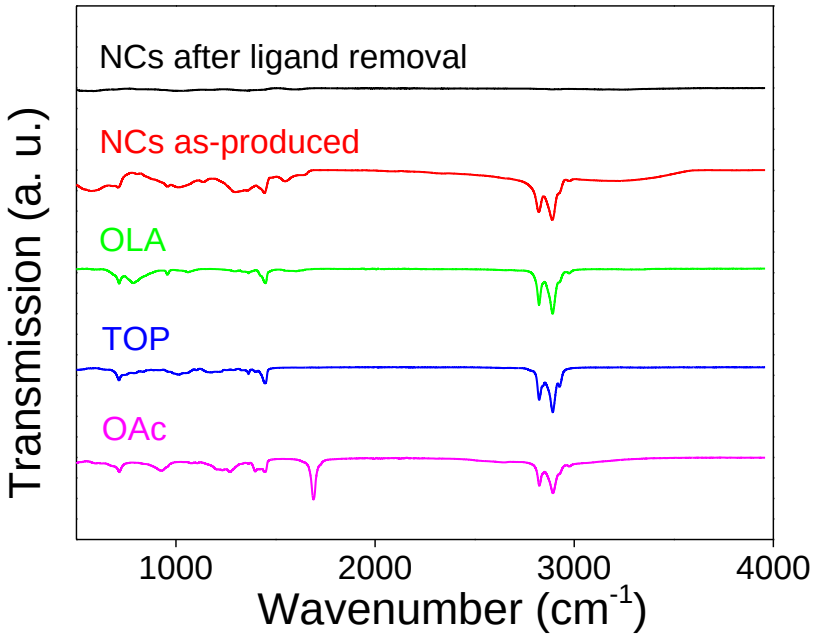

Figure S5. FTIR spectra of OAm, OAc, TOP and $Ni_{3-x}Co_xSn_2$ (x = 0.5) NPs as produced and after ligand removal.

Electrochemical measurements

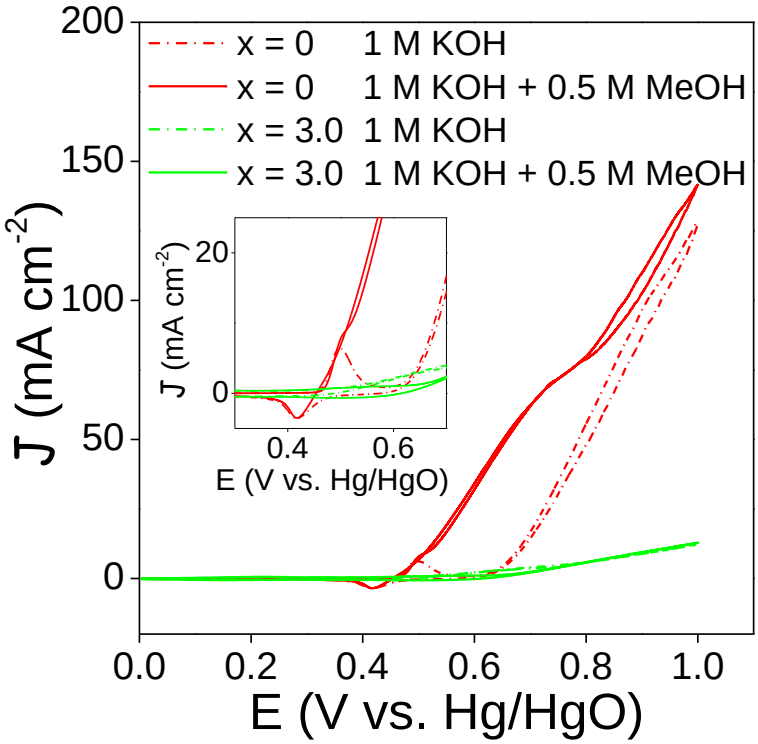

Figure S6. Cyclic voltammograms of $Ni_{3-x}Co_xSn_2$ (x = 0, 3.0) NPs in 1 M KOH solution at a scan rate of 50 mV s^{-1} in the presence and absence of 0.5 M methanol, inset shows an enlarged area of the current density with the applied potential of 0.35-0.65 V.

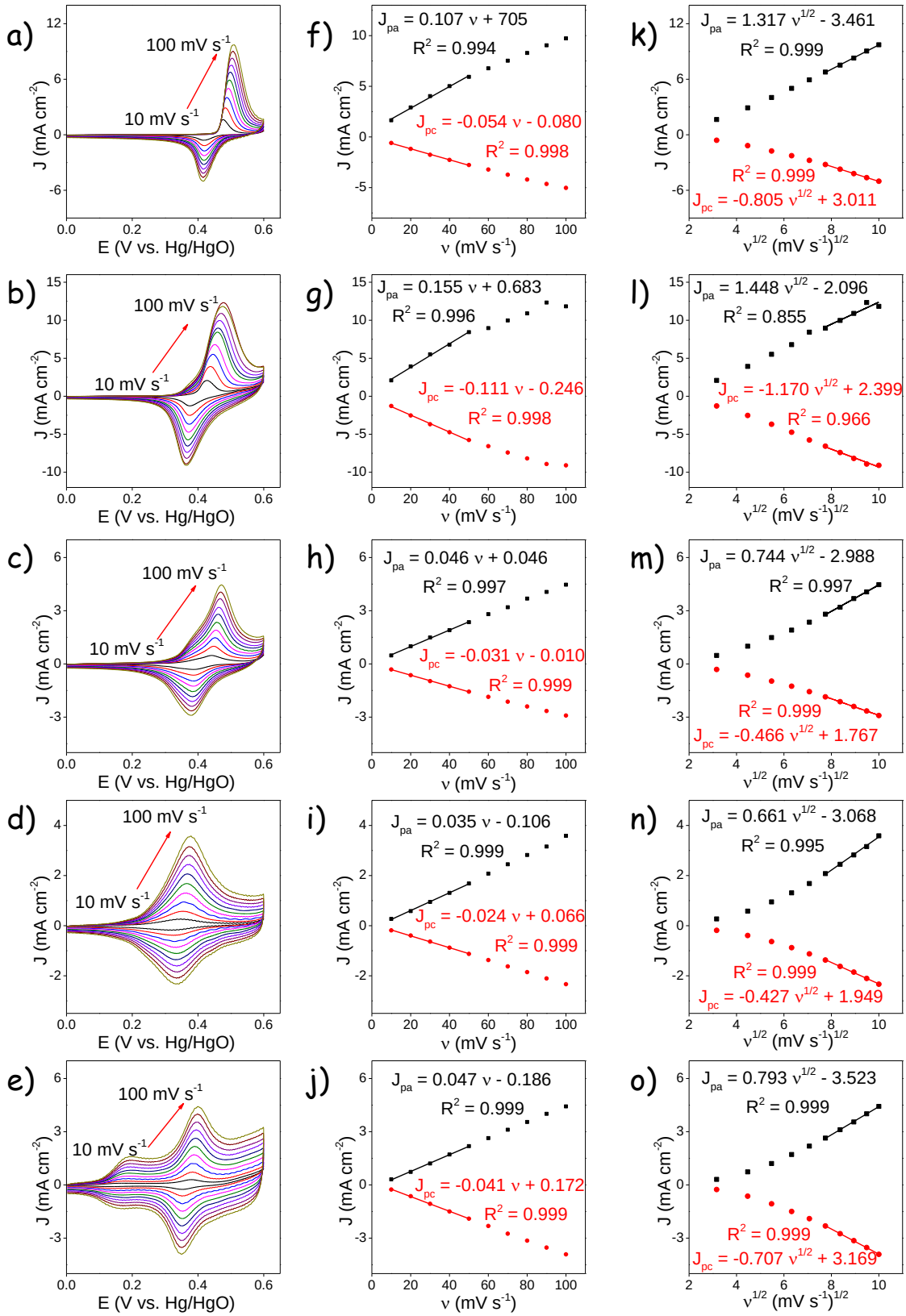

Figure S7. (a-e) Cyclic voltammograms of $Ni_{3-x}Co_xSn_2$ (x = 0, 0.5, 1.0, 2.0, 2.5) NPs in 1 M KOH solution at increasingly higher potentials sweep rates: 10, 20, 30, 40, 50, 60, 70, 80, 90, 100 mVs^{-1}. (f-j) Linear fitting of anodic and cathodic peak current densities to the scan rates of Ni3-xCoxSn2 (x = 0, 0.5, 1.0, 2.0, 2.5) NPs. (k-o)Linear fitting of anodic and cathodic peak current densities to the square roots of the scan rates of $Ni_{3-x}Co_xSn_2$ (x = 0, 0.5, 1.0, 2.0, 2.5) NPs.

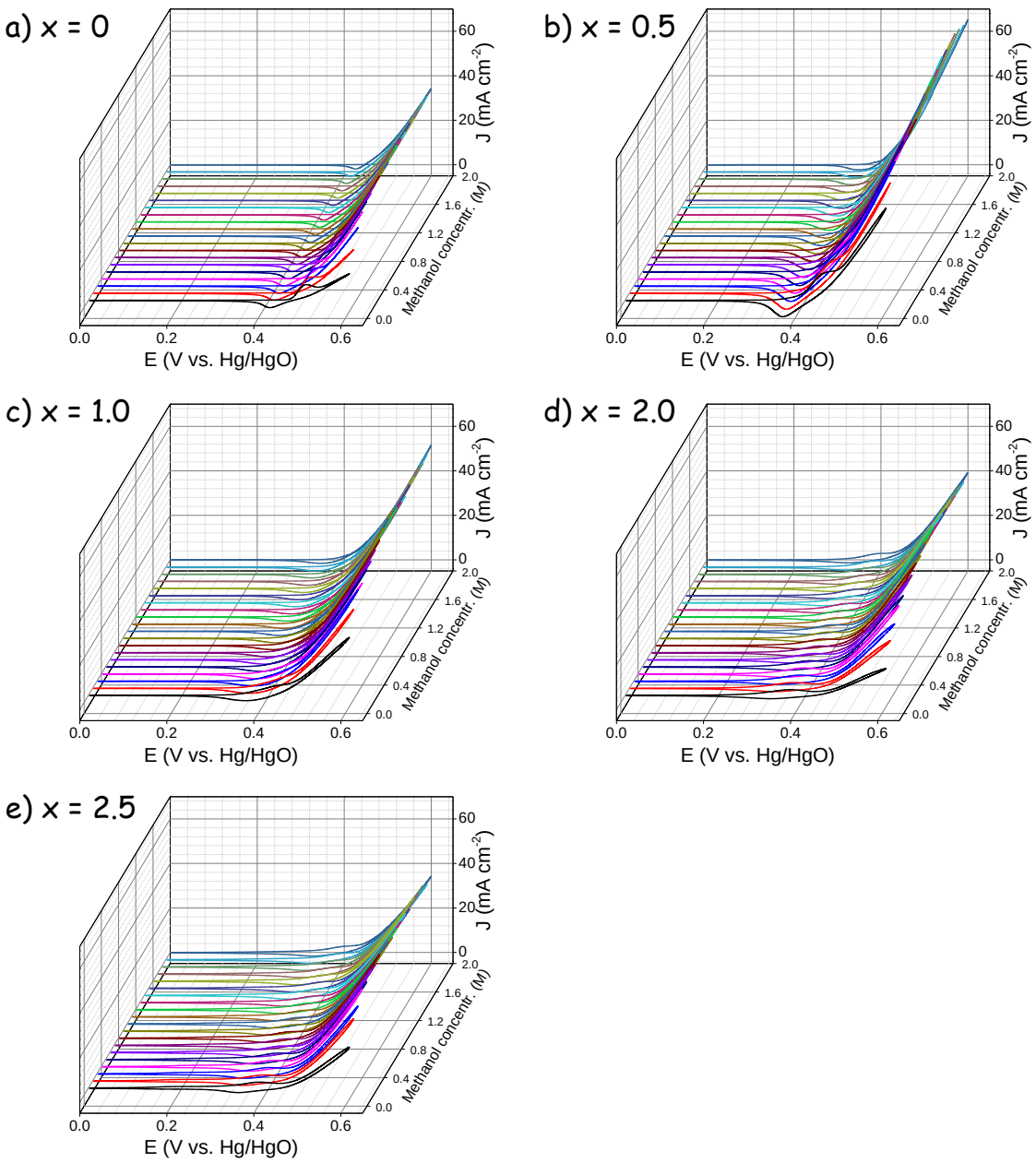

Figure S8. (a-e) CVs of $Ni_{3-x}Co_xSn_2$ (x = 0, 0.5, 1.0, 2.0, 2.5) electrode in 1 M KOH solution with different methanol concentrations from 0.1 M to 2.0 M at a scan rate of 50 mV s^{-1}.

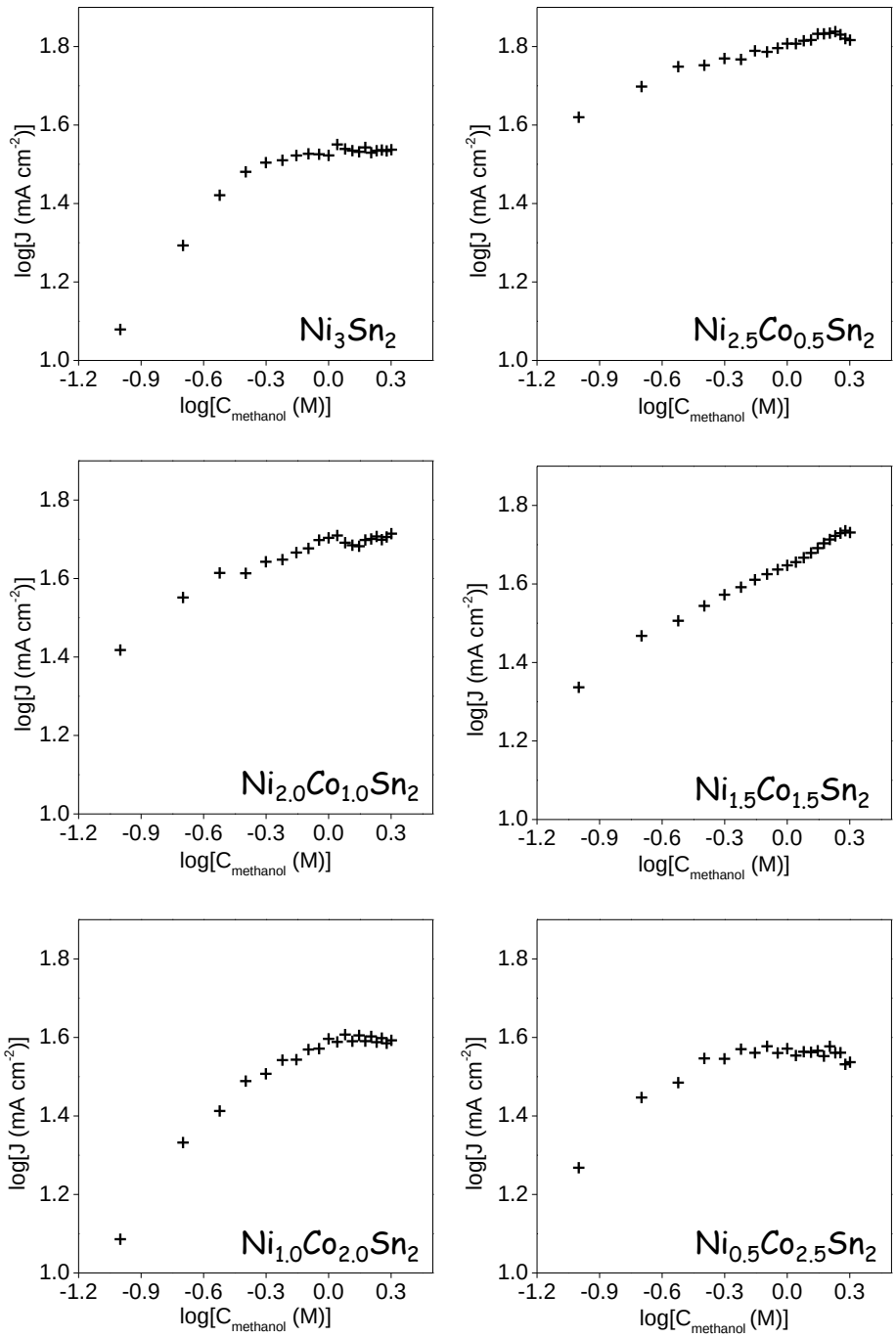

Figure S9. Logarithmic dependence of the current density (0.6 V vs Hg/HgO) for $Ni_{3-x}Co_xSn_2$ ($0\ x \leq 2.5$) electrode with the methanol concentration in 1 M KOH solution with various methanol concentrations from 0.1 M to 2.0 M.

Composition evolution while cycling in KOH

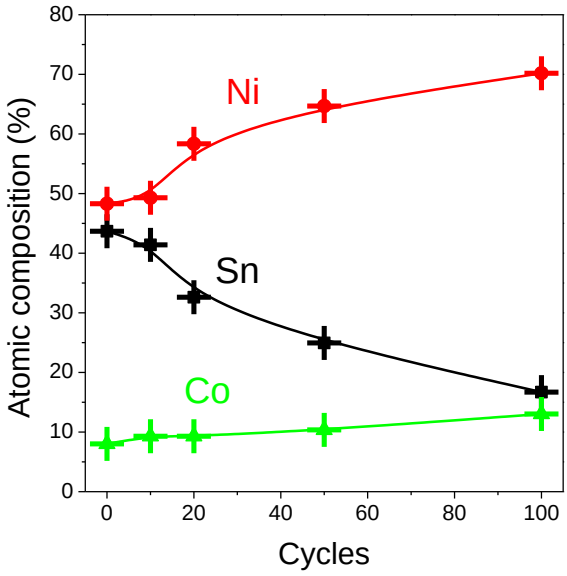

Figure S10. Atomic composition of the $Ni_{2.5}Co_{0.5}Sn_2$ material during CV (0-0.6 V vs Hg/HgO, 50 mV s^{-1}) in 1 M KOH

Computational Details

The calculations were performed using Vienna ab-initio simulation package (VASP).[2–5] The interactions between valence electrons and ion cores were treated by Blöchl's all-electron-like projector augmented wave (PAW) method.[6,7] The exchange-correlation functional was the generalized gradient approximation with the Perdew-Burke-Ernzerhof, known as GGA-PBE.[8] The wave functions at each k-point were expanded with a plane wave basis set and a kinetic cutoff energy up to 400 eV. The electron occupancies were determined according to Fermi scheme with an energy smearing of 0.1 eV. Brillouin zone integration was approximated by a sum over special selected k-points using the Monkhorst–Pack method and they were set to 3×3×1. Geometries were optimized until the energy was converged to 1.0×10^{-6} eV/atom and the force was converged to 0.01 eV/Å. Because of existence the magnetic atom, spin polarization was considered in all calculations. A vacuum layer as large as 20 Å was used along the c direction normal to the surface to avoid periodic interactions.

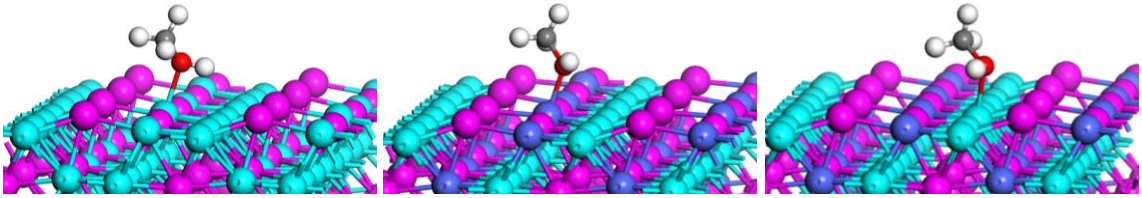

Figure S11. Side view of the absorption of methanol on different atom in (001) surface of Ni_3Sn_2 and $Ni_{2.5}Co_{0.5}Sn_2$ alloy. Green, pink and blue spheres represent Ni, Co and Sn, respectively.

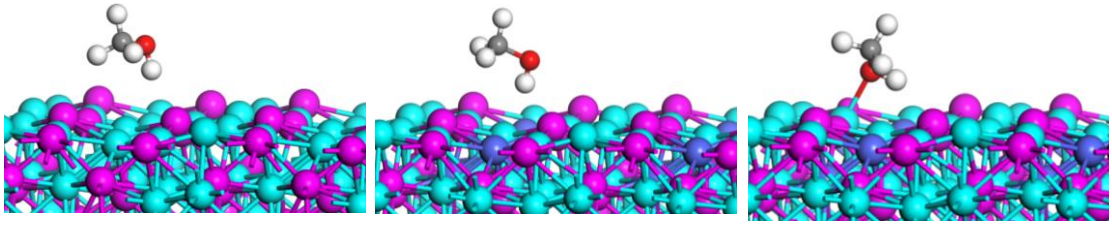

Figure S12. Side view of the absorption of methanol on different atom in (110) surface of Ni_3Sn_2 and $Ni_{2.5}Co_{0.5}Sn_2$ alloy. Green, pink and blue spheres represent Ni, Co and Sn, respectively.

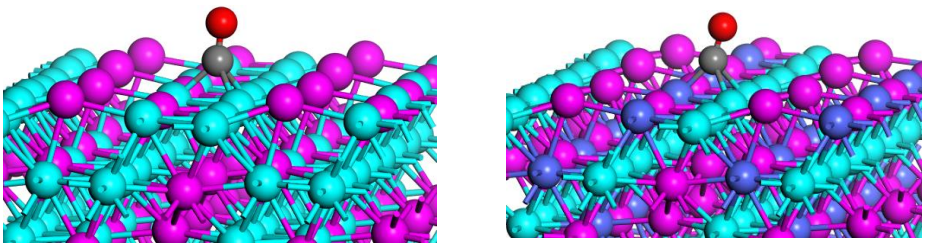

Figure S13. Side view of the absorption of CO in (001) surface of Ni_3Sn_2 and $Ni_{2.5}Co_{0.5}Sn_2$ alloy. Green, pink and blue spheres represent Ni, Co and Sn, respectively.

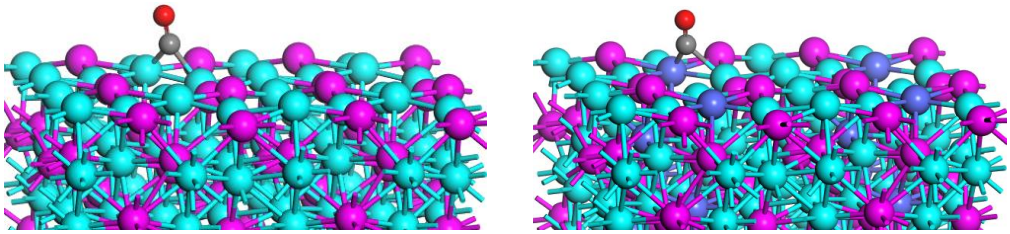

Figure S14. Side view of the absorption of CO in (110) surface of Ni_3Sn_2 and $Ni_{2.5}Co_{0.5}Sn_2$ alloy. Green, pink and blue spheres represent Ni, Co and Sn, respectively.

Comparison of activity

Table S1. Comparison of activity between catalysts in this work and recently reported Ni and Ni-based non-precious metal alloy catalyst

Catalysts	Morphology	Electrolyte	ECSA cm^{-2}	Applied potential V vs. RHE❶	Activity				Reference
					mA cm^{-2} Geometric area	mA cm^{-2} ECSA	mA mg_{metal}^{-1}	ΔJ	
Cu/NiCu/C	Nanowires	1.0 M KOH + 1.0 MeOH		1.55	34.9		867.1	-12%@1000 cycles	9
$Ni_{0.75}Cu_{0.25}$	Branched 3D networks	1.0 M NaOH + 0.5 MeOH	112.5	1.69	84	0.75	168		10
Ni	NPs	0.4 M KOH + 1.0 MeOH		1.64	12				11
FeNi	NPs	0.1 M NaOH + 1.0 MeOH		1.56	50		1709		12
Ni@CNTs	Heterostructures	1.0 M KOH + 1.0 MeOH		1.62	~1.5		966		13
Ni_2Co_2	Cauliflower-like	1.0 M NaOH + 0.5 MeOH	72	1.74	~35	0.49			14
$Ni_{0.5}Co_{0.5}$	Porous alloy film	1.0 M NaOH + 0.5 MeOH		1.69	~35				15
Ni	Ti-supported flakes	1.0 M NaOH + 0.5 MeOH		1.74	39				16
Ni-Ti	NPs	0.1 M NaOH + 0.2 MeOH		1.62	0.5 mA				17
Ni	NPs@rGO	1.0 M KOH + 1.0 MeOH		1.64			1600		18
NiMn	Film	1.0 M NaOH + 0.5 MeOH		1.64	~80				19
$Ni_{1.7}Sn$	NPs	0.5 M KOH + 0.5 MeOH		1.65	50.9		819.3		20
$Ni_{2.5}Co_{0.5}Sn_2$	NPs	1.0 M KOH + 1.0 MeOH	21	1.57	65.5	3.12	1070.4	-35%@1500 cycles	This work
Ni_3Sn_2	NPs	1.0 M KOH + 1.0 MeOH		1.57	34.4		562.7		This work
Pt/C*	Commercial	1.0 M KOH + 1.0 MeOH		0.95			710		9

Note: *Commercial Pt/C was included here for comparison.

❶ For comparison, the applied potential was intended to convert to be vs. RHE using the following equation:

$$E_{RHE} = E^0_{Ref} + E_{Ref} + 0.059 \times PH$$

Where E^0_{Ref} is potential of the reference ($E^0_{Ag/AgCl} = 0.21$ V, $E^0_{Hg/HgO} = 0.14$ V), E_{Ref} is the potential that measured vs. reference, PH is simply converted from the electrolyte (PH = 14 + lg[OH^-], [OH^-] is the OH^- concentration of the alkaline media).

Reference

1 C. D. Wager, W. M. Riggs, L. E. Davis, J. F. Moulder and G. E. Muilenderg, *Handbook of X-ray photoelectron spectroscopy*, Perkin-Elmer Corporation Physical Electronics Division, 1979.

2 G. Kresse and J. Furthmüller, *Phys. Rev. B*, 1996, **54**, 11169–11186.

3 G. Kresse and J. Hafner, *Phys. Rev. B*, 1994, **49**, 14251–14269.

4 G. Kresse and J. Hafner, *Phys. Rev. B*, 1993, **47**, 558–561.

5 G. Kresse and J. Furthmüller, *Comput. Mater. Sci.*, 1996, **6**, 15–50.

6 P. E. Blöchl, *Phys. Rev. B*, 1994, **50**, 17953–17979.

7 G. Kresse and D. Joubert, *Phys. Rev. B*, 1999, **59**, 1758–1775.

8 J. P. Perdew, K. Burke and M. Ernzerhof, *Phys. Rev. Lett.*, 1996, **77**, 3865–3868.

9 D. Wu, W. Zhang and D. Cheng, *ACS Appl. Mater. Interfaces*, 2017, **9**, 19843–19851.

10 X. Cui, P. Xiao, J. Wang, M. Zhou, W. Guo, Y. Yang, Y. He, Z. Wang, Y. Yang, Y. Zhang and Z. Lin, *Angew. Chemie Int. Ed.*, 2017, **56**, 4488–4493.

11 R. M. Abdel Hameed and R. M. El-Sherif, *Appl. Catal. B Environ.*, 2015, **162**, 217–226.

12 S. L. Candelaria, N. M. Bedford, T. J. Woehl, N. S. Rentz, A. R. Showalter, S. Pylypenko, B. A. Bunker, S. Lee, B. Reinhart, Y. Ren, S. P. Ertem, E. B. Coughlin, N. A. Sather, J. L. Horan, A. M. Herring and L. F. Greenlee, *ACS Catal.*, 2017, **7**, 365–379.

13 J. Wang, D. Teschner, Y. Yao, X. Huang, M. Willinger, L. Shao and R. Schlögl, *J. Mater. Chem. A*, 2017, **5**, 9946–9951.

14 X. Cui, W. Guo, M. Zhou, Y. Yang, Y. Li, P. Xiao, Y. Zhang and X. Zhang, *ACS Appl. Mater. Interfaces*, 2015, **7**, 493–503.

15 X. Cui, Y. Yang, Y. Li, F. Liu, H. Peng, Y. Zhang and P. Xiao, *J. Electrochem. Soc.*, 2015, **162**, F1415–F1424.

16 Q. Yi, W. Huang, J. Zhang, X. Liu and L. Li, *Catal. Commun.*, 2008, **9**, 2053–2058.

17 Y. Yu, Q. Yang, X. Li, M. Guo and J. Hu, *Green Chem.*, 2016, **18**, 2827–2833.

18 H. Sun, Y. Ye, J. Liu, Z. Tian, Y. Cai, P. Li and C. Liang, *Chem. Commun.*, 2018, **54**, 1563–1566.

19 I. Danaee, M. Jafarian, A. Mirzapoor, F. Gobal and M. G. Mahjani, *Electrochim. Acta*, 2010, **55**, 2093–2100.

20 J. Li, Z. Luo, Y. Zuo, J. Liu, T. Zhang, P. Tang, J. Arbiol, J. Llorca and A. Cabot, *Appl. Catal. B Environ.*, 2018, **234**, 10–18.